Solid State Ionics 317 (2018) 214–220

Contents lists available at ScienceDirect

Solid State Ionics

journal homepage: www.elsevier.com/locate/ssi

Milling effect on the local structure, site occupation, and site migration in aluminum substituted lithium manganese oxides

Koichi Nakamura[a,*], Kosuke Shimokita[b], Yoichi Sakamoto[b], Kuniyuki Koyama[a], Toshihiro Moriga[a], Naoaki Kuwata[c], Yoshiki Iwai[c], Junichi Kawamura[c]

[a] Graduate School of Technology, Industrial and Social Sciences, Tokushima University, Minami-Josanjima-Cho 2-1, Tokushima 770-8506, Japan
[b] Graduate School of Advanced Technology and Science, Tokushima University, Minami-Josanjima-Cho 2-1, Tokushima 770-8506, Japan
[c] Institute of Multidisciplinary Research for Advanced Materials, Tohoku University, Katahira 2-1-1, Aobaku, Sendai 980-8577, Japan

ARTICLE INFO

Keywords:
$LiMn_2O_4$
Al substitution
NMR
Electrical resistivity
Li^+ ion migration

ABSTRACT

^7Li and ^{27}Al MAS-NMR, magnetic susceptibility, and complex impedance measurements have been performed to study the local structure and electrical resistivity in Al doped spinel $LiMn_{2-x}Al_xO_4$ ($x = 0$, 0.05) exposed to a ball-milling process. The milling process decreased the effective magnetic moment of the Mn species, arising from the appearance of Mn^{4+}, and lead to the suppression of the antiferromagnetic correlation. A hopping time and an activation energy for hopping charge carrier, estimated from electrical resistivity, relatively became larger above milling time of 2.5 h. ^7Li and ^{27}Al MAS-NMR spectra were dependent on milling time, and changes in the spectrum intensities were related to the distribution of Al/Li site occupation. Consequently, we concluded that structural disorder caused by the moderate milling process stimulated a migration of Al^{3+} ions from the 8*a* site to the 16*d* one and the increase of Li^+ ions at the 8*a* site on the diffusion pathway. Such a mutual site migration between the 8*a* and 16*d* site for Li^+ and Al^{3+} ions would be favorable to Li^+ ion diffusion in the milled samples.

1. Introduction

Lithium manganese spinel, $LiMn_2O_4$, is one of promising candidates for electrode materials of lithium rechargeable batteries. It has a high energy capacity per unit weight, is low cost and non-toxicity, hence it is environmentally friendly. It is expected as a replaceable electrode material for a commercial material such as $LiCoO_2$. In this spinel compound and substituted spinel systems, however, some problems, for instance, relatively low capacity (~120 mA h/g) and fading upon cycling need to be improved for application to commercial electrode materials [1–7]. The crystal structure of $LiMn_2O_4$, belongs to a cubic system with space group $Fd\bar{3}m$, in which Li^+, $Mn^{3+/4+}$, and O^{2-} ions are located in the tetrahedral 8*a*, octahedral 16*d*, and 32*e* sites, respectively, as shown in Fig. 1. A Li^+ ion migrates between the 8*a* sites via the 16*c* interstice, which is located in the unoccupied octahedral position neighboring tetrahedral Li 8*a* one [8–11].

Electrical conductivity studies have revealed that $LiMn_2O_4$ is a small polaron semiconductor because of unpaired e_g electrons on Mn^{3+} sites, which are trapped in local lattice relaxation sites [12–16]. Electrical conductivity is 1.9×10^{-5} S/cm at room temperature and an activation energy is 0.16 eV from analyzing electron hopping mechanism between Mn^{3+} and Mn^{4+} ions [15]. Chemical diffusion coefficient of Li in $LiMn_2O_4$ is represented as $D = 2.5 \times 10^{-5}\exp(-0.26/k_BT)$, and a main contribution to the electrical conduction in $LiMn_2O_4$ is not a Li^+ ion conductivity, but a small polaron conductivity [16].

The Jahn-Teller distortion arising from a Mn^{3+} ($t_{2g}^3e_g^1$) state is closely related to capacity fade of a stoichiometric $LiMn_2O_4$, because it directly disturbs the Li^+ ionic conduction pathway. Therefore, substitution effect for the typical Jahn-Teller active Mn^{3+} ion has been widely studied to suppress the Jahn-Teller distortion in $LiMn_2O_4$ [17–20]. Substitution for the Mn^{3+} ion effectively degrades the Jahn-Teller interaction and reinforces the chemical bonding between transition-metals and oxygen ions [21, 22]. On the other hand, it is also reported that such a doping often causes a degradation of the initial discharge capacity [23, 24]. Therefore, it is important to understand changes in local structure and Li^+ ion migration in the impurity doped $LiMn_2O_4$ system.

NMR technique is a powerful tool to probe local structure around observed nucleus and electronic state of ions. So far, NMR studies on local structure have been performed; a ^6Li NMR peak position in $Li_xMn_2O_4$ sensitively shifts with a decrease in Li content, and a new peak, which is assigned to Li^+ ion occupying the 8*a* site in a Mn^{4+} rich

* Corresponding author.
E-mail address: nakamura.o.koichi@tokushima-u.ac.jp (K. Nakamura).

https://doi.org/10.1016/j.ssi.2018.01.019
Received 8 September 2017; Received in revised form 13 January 2018; Accepted 15 January 2018

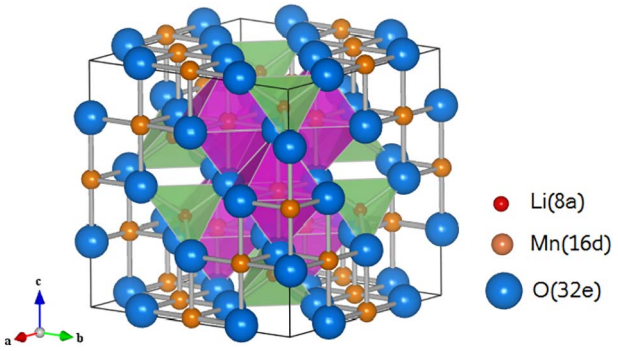

Fig. 1. Crystal structure of $LiMn_2O_4$. Solid lines show a unit cell.

phase, appears at around 950 ppm for $x < 0.3$ [25]. A single resonance peak is dominant in a normal cubic phase in $LiMn_2O_4$ prepared at 850 °C, while several peaks associated with Mn^{4+} are observed in the NMR measurement and no evidence for the Jahn-Teller distortion is observed in a sample containing considerable disorder prepared at relatively low temperature [26]. Doped Al ions occupy not only a six-fold coordinated Mn site, but also a four-fold coordinated Mn site in the Al doped $LiMn_2O_4$. Analysis of ^{27}Al NMR spectrum has revealed that a ratio of distribution for six-fold and four-fold Al is 85%:15% [19]. In addition, some insights in the Li ion dynamics have been probed with regard to spinel systems; a 2D ^{7}Li-NMR measurement reveals the Li^+ ion exchange between the 8*a* and the 16*c* site in $LiMn_2O_4$ with an activation energy of 0.5 eV [27]. In cubic spinel $Li_4Ti_5O_{12}$, ultraslow Li diffusion, which is dependent on the Li transport length scale, is observed in the spin–lattice relaxation measurement [28].

The ball-milling is extensively utilized to induce the disorder such as defects and dislocation in solids by a confliction energy between small hard balls and particles of sample materials. The structural disorder induced in crystal structure would affect a stability of crystal structure and bonding to surrounding ions. Indeed, they would cause changes in an activation energy and conducting behaviors in some dielectric lithium oxides [29, 30]. It is anticipated that such a structural change stimulates the Li^+ ion motion and leads to an enhancement of electrical conduction in the Al doped $LiMn_2O_4$.

In this paper, we discuss milling effect on structural change, site migration, and electrical conductive behavior in $LiMn_{2-x}Al_xO_4$ ($x = 0$, 0.05) based on results of ^{7}Li and ^{27}Al MAS NMR and electrical resistivity measurements.

2. Experimental

Al substituted $LiMn_2O_4$ was prepared by solid state reaction method. The mixture of powdered Li_2CO_3, MnO_2, and $Al(OH)_3$ weighted in a molar ratio of Li:Mn:Al = 1:2 − *x*:*x* was mechanically mixed for 40 min and was sintered at 750 °C for 72 h after sintering at 350 °C for 4 h in air. Finally, we obtained polycrystalline samples of $LiMn_2O_4$ (abbreviated as LMO) and $LiMn_{1.95}Al_{0.05}O_4$ (abbreviated as LMA5). The obtained samples were milled with ethanol on a Fritsch planetary ball milling machine P-6 for 1.25–20 h at a rotation speed of 600 rpm. A zirconia pot (inner volume of 30 ml) and zirconia balls (2 mm in diameter) were used. A weight ratio of sample to ball was 1:15 in the milling process.

Sample characterizations were performed using XRD, chelatometric titration, and iodometric one. XRD measurements were performed using a RINT 2000 HV with Cu Kα1 X-ray (40 kV, 100 mA). Chelatometric titration was performed to determine amount of Mn ion with a back titration method in a 1 M Mg-EDTA (Ethylenediaminetetraacetic acid) solution and a H_4Cl-NH_3 buffer solution (pH 10).

Magnetic susceptibility χ, which is sensitive to the valence of the electronic state of $Mn^{3+/4+}$, was measured using a SQUID magnetometer (Quantum Design MPMS) in the temperature range from 2 to 300 K under a magnetic field of 10^4 Oe.

Complex impedance measurement was performed on a computer controlled HP-4192A impedance analyzer. The powder sample was compressed at 1000 kg/m^2 in a glass ceramic ring cell (10 mm in inner and 20 mm in outer diameter). After compressed, the pellet with the ring was held between two spring-loaded stainless steel electrodes (20 mm in diameter) and mounted in an electric furnace. The measurements of the pellet were performed in a frequency range from 50 Hz to 5 MHz to avoid scattering of data at low frequency and a temperature range from 293 to 573 K. The complex electrical resistivity ρ* ($=\rho' + i\rho''$) was calculated from impedance $|Z^*|$ and phase θ.

MAS-NMR measurements for ^{7}Li ($I = 3/2$, $\gamma = 16.547$ MHz/T) and ^{27}Al ($I = 5/2$, $\gamma = 11.094$ MHz/T) were performed on a Bruker Avance 600 at 233.2 and 156.3 MHz and on a Bruker Avance 300 at 116.6 and 78.2 MHz, respectively. Powdered sample was packed into a zirconia rotor (2 mm or 4 mm in diameter). The magic angle spinning was operated up to 30 kHz. A single pulse sequence was used. 1.0 M LiCl aqueous solution and $Al(NO_3)_3$ saturated solution were used as references for ^{7}Li and ^{27}Al, respectively.

3. Experimental results

3.1. Crystal structure and valence of Mn

The reflection peaks in XRD patterns of the milled LMO and LMA5 became broader with an increase in milling time and were mainly identified as a cubic spinel structure with the space group of $Fd\bar{3}m$ as shown in Fig. 2(a) and (b). The split peaks at around 64° as shown in insets of Fig. 2(a) and (b), consisting of reflection peaks from the cubic spinel phase and tetragonal phases (represented respectively by an asterisk and an open triangle), were observed in LMA5 as well as LMO [31]. The lattice parameter of the cubic phase in LMO showed a tendency to decrease as milling time increased as shown in Fig. 2(c). LMO and LMA5 showed no significant change in lattice constant above 10 h of milling. LMO with oxygen deficiency shows a similar decrease in lattice parameters as reported in a previous study [20]. It is be attributed to an increase in the effective valence from Mn^{3+} with a larger ionic radius to Mn^{4+} with a smaller one with an increase in milling time [20,32]. On the other hand, lattice parameters of LMA5 increased up to 2.5 h of milling and was close to that of LMO above 2.5 h. An increase in lattice parameter observed in the milled LMA5 sample would be associated with the changes in the Al coordination as mentioned later. It is known that the ionic radius of the six-fold Al^{3+} ion is larger than that of four-fold Al^{3+} ion [32]. The number of the six-fold coordinated Al^{3+} ion would increase with an increase in milling time.

Iodometry and Cheletometric titration showed that the Mn content of the non-substituted LMO decreased, evaluated to be 1.97, 1.94, and 1.89 for 0, 2.5 and 10 h, respectively, as milling time increased. The Mn valence increasd with an increase in milling time and oxygen deficiency showed a minimum value at 2.5 h. In this milling process the Mn valence changes as $2Mn^{3+} \rightarrow Mn^{2+} + Mn^{4+}$. Then, an increase of Mn^{2+} in solution in ethanol resulted in an increase of Mn^{4+} and a decrease of Mn^{3+} in LMO. The effective valence of Mn increased from +3.31 to +3.50 upto 10 h of milling.

3.2. Magnetic susceptibility

Magnetic susceptibility revealed the changes of the electronic state of $Mn^{3+/4+}$ species with milling. Fig. 3 shows the temperature dependence of the magnetic susceptibility χ of LMA5 exposed to 0, 2.5, and 10 h. The inverse of χ is proportional to temperature above 150 K as shown in an inset, indicating that the temperature dependence of χ follows Curie-Weiss law